Book ISBN: 978-952-412-288-7 | Series ISSN 2709-7609 (Online) | License: CC BY-NC-ND 4.0 | Pages: 11

DEVELOPMENT AND VALIDATION OF A MEAN-LINE CODE FOR DESIGN OPTIMIZATION AND OFF-DESIGN ANALYSIS OF ORGANIC RANKINE CYCLE AXIAL TURBINES

Marco Oliveti[1*], Giacomo Persico[1]

[1] *Politecnico di Milano, Department of Energy, 20156, Milano, Italy*

* Corresponding Author: marco.oliveti@polimi.it

ABSTRACT

Optimisation of expander performance is a critical factor in improving the overall profitability of Organic Rankine Cycles (ORC) systems. Low-fidelity tools, such as mean-line codes, play a fundamental role in the preliminary design phase by balancing computational efficiency and accuracy. Leveraging on the original in-house zTurbo software, this paper introduces an advanced Python-based mean-line code for multistage axial turbines operating with organic fluids. The classical Traupel loss correlations have been replaced by Aungier's more recent model, which better reproduces the performance of advanced turbomachinery designs used in present-day ORC turbine technology. The code significantly improves computational efficiency and incorporates a genetic algorithm to optimise design parameters, maximising the efficiency within specified constraints. A key novelty of this work is the introduction of a dedicated off-design analysis capability. This new version of the code enables the evaluation of turbine performance under varying operating conditions, which is crucial for ORC turbines in applications like geothermal energy and waste heat recovery, where operating conditions can fluctuate significantly. The enhanced code has been systematically assessed through comparisons with higher fidelity computational fluid dynamics simulations under in design and off-design conditions. Results confirm the robustness of the Aungier loss correlations and the accuracy of the code across various working conditions. By addressing both design and off-design performance, the developed software demonstrates its potential as a reliable and versatile tool for the preliminary design and optimisation of ORC axial turbines.

1. INTRODUCTION

The relevance of the expander efficiency in Organic Rankine Cycle (ORC) systems has been widely recognised in the literature (Macchi, 2017; Jiménez-García *et al.*, 2023). Due to the lack of standardised turbine designs and the broad range of possible working fluids, many applications require a flexible design approach where multiple parameters need to be defined and optimised (Haghighi *et al.*, 2020). Given the complexity of this process, low-fidelity methods, such as 1D mean-line codes, are commonly employed to provide a preliminary definition of the expander while balancing computational efficiency and predictive accuracy. However, the limited availability of experimental data for ORC turbines implies that most loss correlations found in the literature were originally developed for gas and steam turbines operating with conventional working fluids. As a result, many existing mean-line tools have not been systematically validated for ORC-specific applications. This work presents the development of an accurate and efficient mean-line code specifically conceived for design and analysis of multi-stage axial ORC turbines. This expander architecture is preferred for mid-to-high power applications, such as geothermal energy and waste heat recovery (Mahmoudi *et al.*, 2018), due to its ability to handle high mass flow rates and expansion ratios. The novelty of the work lies in the integration of more advanced loss correlations, specifically those proposed by Aungier (Aungier, 2006), to improve accuracy in transonic conditions, common in most ORC turbines. In addition, the software incorporates an off-design analysis

capability, allowing reliable performance predictions across a range of operating conditions. A further original aspect is the direct coupling of the mean-line solver with a genetic algorithm, enabling robust optimisation of the turbine configuration at the design stage. The combination of these features makes the tool particularly suited to address the specific design and analysis needs of ORC axial turbines. Due to the absence of experimental data for multistage ORC turbines in open literature, the code is compared against numerical results obtained through CFD 3D simulations.

Section 2 describes the main features of the code, focusing on the algorithm structure, and on the strategies exploited for both design optimization and off-design prediction. A brief description of the selected loss correlations is provided and an overview on the integration of the code in a genetic optimizer is presented. In Section 3 the selected case study for the analysis is reported, followed by a systematic comparison between mean-line results and CFD simulations.

2. CODE DEVELOPMENT

2.1 Code Structure

The mean-line code has been developed in Python to take advantage of built-in numerical solvers, incorporate CoolProp (Bell *et al.*, 2014) for thermodynamic property calculations, and facilitate its integration with a genetic algorithm for optimisation (see Section 2.3). This section first outlines the structure of the design algorithm and then details the modifications required for off-design analysis.

First, the input quantities are read and stored in a dictionary structure. This dictionary contains all turbine variables, which are progressively defined during execution as 4-by-N matrices, where N is the number of turbine stages and each matrix row represents the stator and rotor inlet and outlet conditions. The required input quantities for the design code can be categorised as follows:

- Thermodynamic quantities: inlet total temperature and pressure, outlet static pressure, mass flow rate, expansion ratio of each stage.
- Kinematic quantities: inlet flow angle, rotational speed.
- Geometric quantities: axial chords, inlet hub-to-mean diameter ratio (h_b/D), inlet loading coefficient, trailing edge-to-throat width ratio (te/o), tip clearances, outlet geometric angles.
- Additional parameters: reaction degrees, number of stages, working fluid.

Once the input data is stored, the thermodynamic model is initialised. To account for fluid non-ideality, the Refprop (Lemmon *et al.*, 2018) fluid library is accessed via the CoolProp low-level Python wrapper. This initializes an abstract state object that is updated whenever two static or total properties are specified at a given station, allowing all other properties to be computed accordingly. An alternative version of the code uses look-up tables for thermodynamic properties. This approach, generally slower for pure fluids, becomes more convenient in the case of complex mixtures where CoolProp calculations require longer computational time or if a particular mixture is not available in the fluid library.
The mean diameter, assumed constant in the current implementation, is determined from the inlet loading coefficient, enabling the calculation of inlet velocity and static conditions. Each stage is then solved inside an iterative cycle, where the stator and then the rotor are characterized through the computations in the algorithm whose block diagram is reported in Figure 1. In the design code, the isentropic expansions

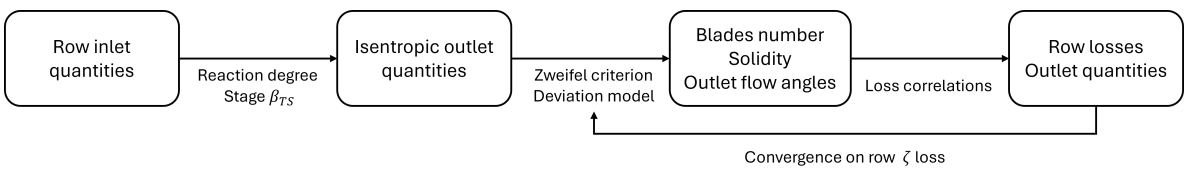

Figure 1: Block diagram of the algorithm for the solution of each turbine row

are derived through the conservation of total enthalpy in the stator and rothalpy in the rotor, as both the total-static expansion ratio and the stage reaction degree are known. Once the isentropic outlet state is obtained, this serves as the initial guess for an iterative process where the Zweifel criterion (Zweifel, 1945) is used to compute the optimal solidity and the blade number of the row. Loss correlations are then applied to estimate outlet flow angles and cascade losses and therefore determining the blade heights. At the end of each iteration, the row performances are evaluated through the loss coefficient

$$\zeta = \frac{h_1 - h_{1,is}}{v_{1,is}^2} \tag{1}$$

iterating up to its convergence with a tolerance of 10^{-6}. Once the losses are determined, total and static quantities downstream of the cascade are obtained, allowing the computation to proceed to the next row up to the last rotor. Finally, the turbine design data are stored in an output file containing all the thermodynamic, kinematic, and geometric losses, as well as the meridional section of the expander and the corresponding velocity triangles.

The off-design module builds upon the same code architecture as the design tool but operates with a different set of input data. In this case, the turbine geometry is fully defined, while key operational parameters, such as the mass flow rate, the reaction degree of each stage, and the expansion ratio distribution, are unknowns to be determined. The turbine geometry is read from the design output file, while the other data are used as initial estimates for the unknowns. Additionally, the new boundary conditions must be specified, either as absolute values or as variations in inlet or outlet pressure and temperature.

As in the design code, losses are evaluated through an iterative procedure, starting with an isentropic calculation followed by successive corrections using the loss model until convergence is reached on the cascade performance. However, in off-design conditions, the mass flow rate and the stage expansion ratios are unknown, requiring an additional outer iteration loop to enforce mass conservation. This is achieved using the procedure devised by Came (Came, 1995), as illustrated by the algorithm block diagram in Figure 2.

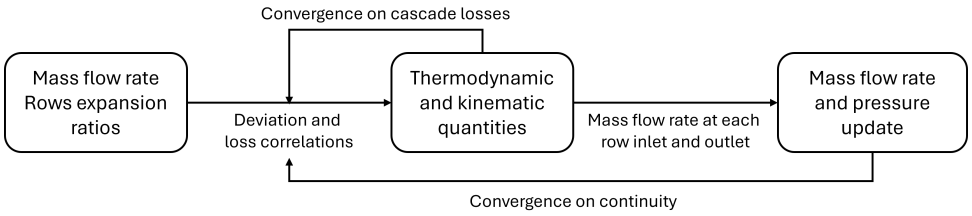

Figure 2: Came's target pressure algorithm block diagram

Initial estimate for the mass flow rate is taken from the design output file, while the expansion ratio is, at first, equally distributed across every row. The turbine performance is then computed iteratively until convergence is reached. Since mass imbalance occurs between different cascades, the mass flow rate is iteratively adjusted based on the value computed at the first stator outlet. To improve numerical stability and ensure convergence, relaxation factors are applied to prevent excessive updates. At the end of each iteration i, the mass flow rate at the station j is computed as:

$$\dot{m}_{check}^{i,j} = [\rho v_a A]^{i,j} \tag{2}$$

This value is then used to calculate the updated mass flow rate used for the following iteration, which is:

$$\dot{m}^{i+1} = \dot{m}^i + k_m(\dot{m}_{check}^{i,\,\text{I stator}} - \dot{m}^i) \tag{3}$$

with k_m being the mass flow rate relaxation factor, usually fixed at 0.75. The pressure distribution is then updated at each iteration according to:

$$P^{i+1,j} = (1-k_p)P^{i,j} + k_p P^{i,j} \frac{\dot{m}^i + k_m(\dot{m}^{i,j}_{check} - \dot{m}^i)}{\dot{m}^{i,j}_{check}} \tag{4}$$

where k_p is the pressure relaxation factor, also set at 0.75. The iterative cycle stops when convergence is reached on the mass flow rate, through an evaluation at every iteration of the norm of the vector $\dot{m}^i_{check} - \dot{m}^i$. A plot of these residuals for one of the off-design cases later analysed is reported in Figure 3, where each line represents the difference between the local mass flow rate computed at the outlet of every row and the value of m^i along the code iterations.

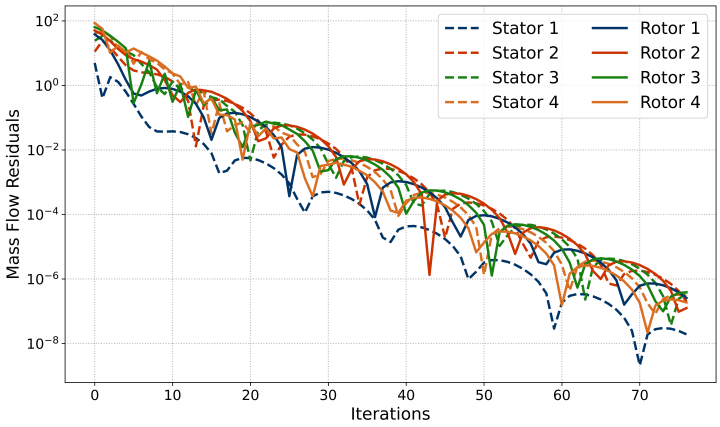

Figure 3: Off-design code mass flow residuals

2.2 Loss Correlations

Both the design and off-design codes rely on Aungier's deviation and loss correlations for axial turbines. This empirical model synthesizes and refines three fundamental performance prediction methods: those developed by Ainley and Mathieson (Ainley and Mathieson, 1951), Dunham and Came (Dunham and Came, 1970), Kacker and Okapuu (Kacker and Okapuu, 1982). Aungier's model was selected for this study as it was specifically developed to handle severe off-design conditions while also improving and extending the original correlations to better represent modern steam turbines, which often feature higher expansion ratios. Additionally, refinements from other performance prediction methods, such as Reynolds number corrections from Craig and Cox (Craig and Cox, 1970), have been incorporated to enhance its applicability. Aungier's loss model accounts for flow path total pressure losses, parasitic losses, and leakage flows. However, since the objective of the mean-line code is to provide a preliminary estimation of the expander flow path performance, parasitic losses and leakage flows have not been considered in the present study. Instead, the focus is placed on the characterization of the flow path total pressure loss coefficient, which Aungier defines as

$$Y = \frac{P_{T1} - P_{T2}}{P_{T1} - P_1} = Y_P + Y_S + Y_{CL} + Y_{TE} + Y_{EX} + Y_{SH} \tag{5}$$

where each term represents a different loss contribution: profile (Y_P), secondary flow (Y_S), clearance (Y_{CL}), trailing edge (Y_{TE}), supersonic expansion (Y_{EX}), and shock losses (Y_{SH}). Each loss component in Aungier's model is computed based on empirical correlations, and the reader is referred to the original work for their complete formulation and derivation. Here, only a few key aspects, particularly those relevant to the present study, are highlighted.

A notable feature of the profile loss model is the inclusion of a modernity factor, introduced by Kacker and Okapuu, which accounts for advancements in blade design. This factor reduces Y_P for optimized

cascades through a multiplicative coefficient smaller than unity. In the results later reported, this was set, as proposed by Aungier, to 0.67. Additionally, the profile loss includes a correction for incidence effects via the coefficient K_{inc}, which plays a crucial role in off-design conditions. This coefficient depends on both the flow incidence and the stalling incidence angle. Aungier proposes a correction factor based on solidity, but this was found to be excessively penalizing, leading to unrealistically high sensitivity to loading, as it predicts the occurrence of a stall condition not encountered in real applications. Modern optimized airfoils, in fact, often feature a large leading edge curvature ratio, which is capable of mitigating this phenomenon. For this reason, the correction has been omitted in the present implementation, as supported by the CFD simulation results described in Section 3.3. Finally, Aungier introduces a correction factor applied to the secondary loss component to prevent excessive penalties for cascades with low aspect ratios, which are typical of the first stages of ORC turbines. This correction improves the applicability of the model to ORC turbine designs, ensuring a more accurate loss estimation without overly penalizing such geometries.

As indicated in Figure 1, loss correlations are applied after the outlet flow angles have been determined. Although an exact deviation prediction would require detailed blade geometry, Aungier proposes an empirical model that provides a first estimation. The model assumes zero deviation when the throat Mach number reaches sonic conditions. For subsonic conditions, the deviation is expressed as a function of the gauging angle and the outlet Mach number, while for supersonic conditions, it is derived from mass flow conservation between the throat and the outlet. This formulation ensures continuity across the sonic condition, improving numerical stability and convergence, particularly in cases where the outlet Mach number is close to unity.

2.3 Design Optimization

As previously stated, the design code requires the prior specification of several interdependent parameters, including flow angles, degrees of reaction and stage expansion ratios. Identifying an optimal configuration, where these parameters yield a highly efficient expander while satisfying specific constraints, is particularly challenging due to the large number of variables in multi-stage turbines and their complex interactions. To address this, an optimization routine has been developed. The optimization is performed using a genetic algorithm, specifically the Differential Evolution (DE) method, implemented in Python via the *pygmo* library (Biscani and Izzo, 2020). The design space is defined by setting upper and lower bounds for the optimized parameters: outlet flow angles, degrees of reaction, individual stage expansion ratios, and the inlet loading coefficient. Though the number of variables to be optimised is relatively high, the definition of the design space is simplified by the efficiency of the algorithm. The bounds for each variable do not need to be tightly set around the anticipated optimum, as the algorithm quickly converges towards the most promising region of the design space within the first few generations, effectively reducing the search area.

Additionally, constraints are imposed to ensure the turbine remains physically realizable and within the validity range of the loss correlations. For expanders such as the one presented in the next section, the design constraints include:

- keeping the radius ratio below 1.5, typically to avoid excessive blade twisting;
- limiting flaring to 30°, in order to prevent flow separation at the endwalls;
- ensuring an outlet Mach number below 1.4 in every cascade, avoiding the need for converging-diverging blades;
- restricting the absolute velocity outlet flow angle to 20° in intermediate stages and 5° at the last stage, to minimise residual kinetic energy and improve overall efficiency.

The optimization objective is to maximize turbine efficiency, assuming a recovery of half the kinetic energy downstream of the expander. Constraints are enforced through a penalty approach, strongly reduc-

ing the objective function value for any infeasible designs. The objective function is defined as:

$$\eta_{T\phi} = \frac{h_{T0} - h_{T2}}{h_{T0} - h_{2,is} - \frac{v_2^2}{4}} - K \sum P_i \tag{6}$$

where P_i represents the penalty assigned to each violated constraint, scaled by a factor K to significantly reduce $\eta_{T\phi}$. The key advantage of integrating the optimization directly with the design code is the elimination of input/output operations at each mean-line computation, greatly improving computational efficiency. As a reference, the optimization generating the expander presented in the next section involved the evolution for 200 generations of a population of 50 elements, requiring less than five minutes to converge to the final design.

3. CODE ASSESSMENT

In this section, the reliability of the mean-line code predictions is assessed by comparing its results with CFD simulations. Given the scarcity of experimental data for multistage ORC turbines in the open literature, numerical results serve as the primary reference for evaluating the model's performance. The comparison focuses on key flow properties and efficiency trends across multiple operating conditions, providing insights into the reliability of the implemented loss and deviation models.

3.1 Case Study Selection

The first step in assessing the code's accuracy was defining a test case to design using the described optimization routine. As one of the main areas of interest for ORC cycles is geothermal energy conversion, the selection of the working fluid and boundary conditions was guided by references from the literature on this specific applications (Manfredi *et al.*, 2023). Since a single test case had to be selected, the assessment was carried out using a specific working fluid. However, the code is designed to operate with any ORC axial turbine and its consistency has been verified through optimisation studies involving several machines using different fluids, including hydrocarbons, siloxanes, and refrigerants. The test case turbine operates with isobutane, a common choice for low-temperature binary-cycle systems. The inlet total temperature and pressure were set to 140°C and 25 bar, respectively, representative of typical geothermal heat source conditions. The outlet pressure was determined based on a condensation temperature of 35 °C, assuming a pinch point temperature difference of 15 °C in the condenser. This resulted in a condensation pressure of 4.65 bar. The mass flow rate was chosen to achieve a target power output of 7 MW, supplying a value of 90 kg/s. For off-design performance, a range of outlet temperatures was investigated, reflecting the variation in ambient conditions. Since the geothermal source remains relatively constant, the outlet temperature becomes the key variable, which depends on ambient temperature. As later reported, 11 conditions ranging from -20 °C to +20 °C with respect to the design point were analysed and compared with corresponding CFD data.

Several design choices were then made to balance performance and feasibility. As the number of stages had to be fixed, optimisations were carried out for configurations with up to six stages, ultimately selecting a four-stage arrangement. This choice was made to achieve an expander that, as common for high-power geothermal ORC turbines, operates in slightly subsonic conditions at the design point, reaching choking as soon as higher expansion ratios are imposed. This configuration allows for a comprehensive performance assessment, as it includes a wide range of operating conditions from low loaded subsonic expansions to highly loaded transonic cases. The rotational speed was fixed at 3000 rpm, avoiding the introduction of a gearbox which would reduce overall plant efficiency. The blade degree of reaction was optimized within the range 0.45 - 0.55, enabling the use of the same blade geometry throughout the entire 3D flow path, accepting the onset of a marginal incidence. To allow the loss correlations to be assessed across different aspect ratios, the axial chord was deliberately set to 30 mm for all cascades instead of being optimized. Additionally, the turbine was designed without tip clearances, postponing the validation of leakage losses for future studies.

The expander obtained from the optimization process can be observed in terms of meridional section

from the 3D representation of the flow path created for the CFD analysis and reported in Figure 4b, while the velocity triangles are later reported in Figure 6 when compared to the ones extracted from CFD simulations. The total-static efficiency of the expander is estimated at 94.36%, which is notably high due to the lack of tip clearance losses.

3.2 CFD Analysis

Upon the optimal mean-line design, a fully 3D flow path was constructed for comparative CFD simulations. The blade geometry, belonging to the Politecnico di Milano in-house database and previously employed in ORC turbine studies, was adapted to create cascades that accurately represented the midspan geometry obtained from the mean-line optimization. For each stage, the blade row was iteratively scaled and rotated until the gauging angle, defined as $\arcsin(o/s)$, the pitch and the axial chord matched the values set by the mean-line code. The blade was then extended to the hub and shroud as a purely prismatic blade, a reasonable design choice for turbines with a limited radius ratio, as it simplifies the manufacturing process. To achieve a perfectly prismatic airfoil, the 2D cylindrical blade coordinates ($r\vartheta$ - z) were converted into 3D Cartesian coordinates using the following transformation:

$$\begin{cases} \vartheta = \frac{r\vartheta}{R(z)} \\ x = R(z)\cos(\vartheta) \\ y = R(z)\sin(\vartheta) \end{cases} \tag{7}$$

where $R(z)$ is a spline defining the variation of the hub or shroud radius along the z-coordinate. The resulting 3D flow path is shown in Figure 4. Figure 4a illustrates the midspan blade-to-blade plane,

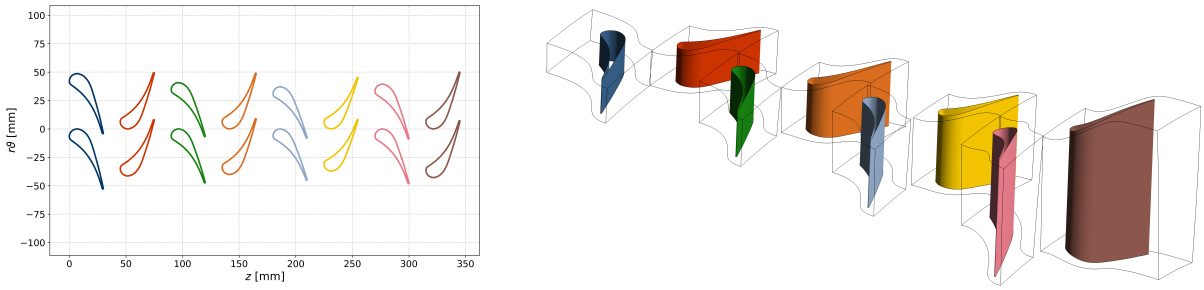

(a) Midspan blade-to-blade plane

(b) 3D flow path

Figure 4: Computational domain definition

while Figure 4b shows the full 3D computational domain. Notice that a gap of half a chord length was introduced between consecutive cascades and that the use of splines for hub and shroud definition ensures continuity and regularity of the endwall shape.

The CFD simulations were conducted using *Ansys CFX*, with mesh generation performed in *Ansys TurboGrid* to ensure a high-quality structured grid. The meshing approach provided fine control over both overall grid density and near-wall resolution, enabling an appropriate y^+ value for the selected turbulence model. The simulations reported here were carried out using the k-ω SST model, requiring an iterative mesh refinement to maintain y^+ around unity. Mixing-plane interfaces were applied between cascades, while periodic boundary conditions were imposed in the pitchwise direction. The outlet pressure is provided through a radial equilibrium distribution, matching the expected outlet pressure at the intermediate blade radius. The high-resolution mesh used in the final calculations, presented in Section 3.3, consisted of approximately 18 million cells.

3.3 Results

The accuracy of the mean-line model in predicting turbine performance is assessed by comparing its results with CFD simulations at both design and off-design conditions. Since the mean-line model provides a single representative value for each quantity, while CFD results exhibit variations in both tangential

and radial directions, a specific post-processing strategy was adopted to ensure a meaningful comparison. First, a circumferential mass-averaging was performed along 16 radial lines placed upstream and downstream of each cascade, spanning from hub to shroud. This allowed the extraction of the radial distribution of flow variables, enabling an initial comparison between the mid-span values predicted by the mean-line model and their actual radial variation in CFD. To obtain a single representative value comparable to the mean-line predictions, a second averaging step was applied, weighting each quantity based on the local mass flux (i.e., ρv_a). This approach was essential for computing global performance indicators such as the expander efficiency.

A first comparison is performed on the enthalpy and pressure distributions along the turbine flow path. These quantities are shown in Figure 5, where CFD results are plotted as radial distributions, while the mean-line values are reported as dots at mid-span. The mean-line model accurately captures the overall trend, even at the stator outlet, where the tangential velocity components induce noticeable radial evolutions in both pressure and enthalpy.

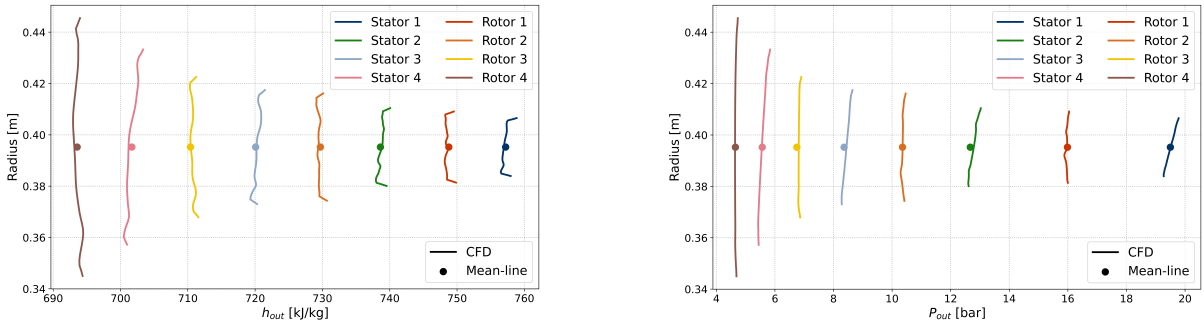

(a) Enthalpy Distribution

(b) Pressure Distribution

Figure 5: Comparison of enthalpy and pressure distribution in design conditions

After assessing the thermodynamic properties, the velocity triangles obtained from the mean-line model and CFD at design conditions are compared. Figure 6 presents an overlay of the velocity triangles at mid-span, highlighting the strong agreement between the mean-line prediction and the 3D simulation. The estimated efficiency at design conditions is also compared between the two approaches. Table 1

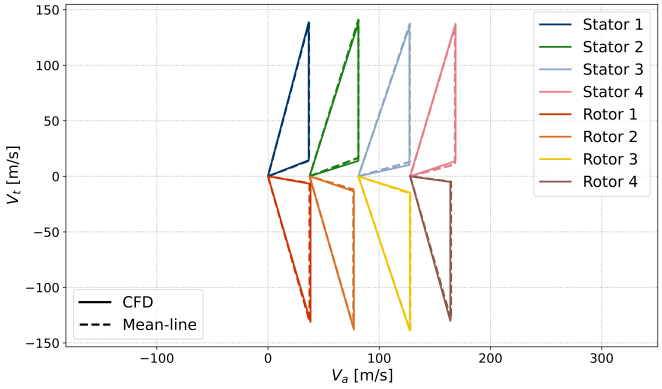

Figure 6: Comparison of velocity triangles at midspan in design conditions

summarizes the values of total-static and total-total efficiencies, showing excellent match between the mean-line model and CFD. Despite the overall accuracy of the mean-line model in estimating thermodynamic and kinematic quantities, a slight overestimation of the mass flow rate is observed. The CFD simulation predicts a mass flow rate approximately 1.5% lower than the design model. Since discrepancies in density are minimal, this deviation is mainly due to a prediction of a higher axial component of

Table 1: Comparison of expander efficiency between mean-line model and CFD in design conditions

	Mean-Line [%]	CFD [%]	Error [%]
Total-Static	94.36	94.44	0.09
Total-Total	95.20	95.26	0.06

the absolute velocity, which, being limited to around 1.5% is not noticeable in the velocity triangles plot in Figure 6.

To assess the reliability of the off-design mean-line prediction, a comparison is performed across the 11 operating points described in Section 3.1. For each case, the condensation pressure was computed based on the ambient temperature and imposed as an outlet boundary condition, maintaining a fixed pinch point of 15°C in the condenser. Total-static and total-total efficiencies were then computed, resulting in the performance maps shown in Figure 7, which show efficiency as a function of ambient temperature. As shown, the mean-line model accurately reproduces the off-design performance, with both efficiency

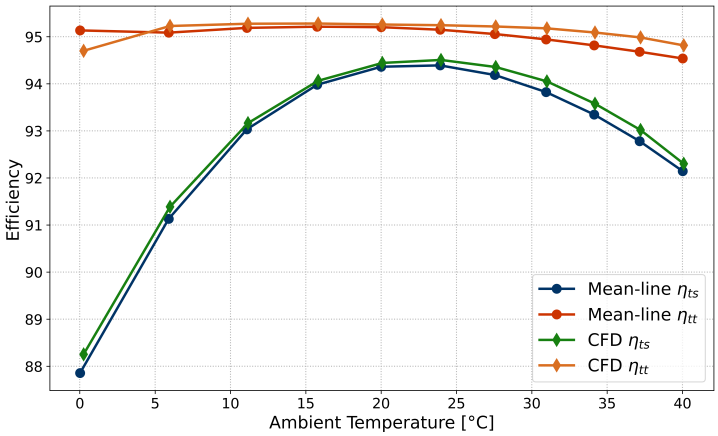

Figure 7: Comparison of efficiency predictions as a function of ambient temperature

curves following an identical trend and exhibiting close values. The discrepancy is slightly larger for total-total efficiency, which, though, becomes less meaningful under off-design conditions, as the assumption of full kinetic energy recovery grows increasingly unrealistic when the diffuser deviates from its design operating point.

An important result of the off-design analysis is the accurate prediction of the pressure ratio distribution across the turbine. At high ambient temperatures, where the expansion ratio is reduced, the loading is redistributed almost proportionally across all stages. On the other hand, where low temperatures lead to a higher expansion ratio, transonic and supersonic flows may occur. A key result is that the mean-line model, through the implementation of Came's target pressure method, correctly identifies the stage where choking occurs. In this case study, choking takes place in the last rotor, where the relative Mach number reaches 1.1 at the outlet. This behaviour leads to a highly uneven redistribution of the expansion ratio, with the last stage experiencing a significant increase in both expansion and loading. The effect is evident in the velocity triangles shown in Figures 8a and 8b for the two extreme cases. In the low-temperature case, the velocity triangles for the first three stages remain almost identical to the design condition, while the fourth stage undergoes a much higher flow deflection and outlet velocity. This is due to the increased expansion ratio and the onset of transonic conditions in the rotor. Conversely, in the high-temperature case, the expansion ratio is more evenly distributed across all stages, resulting in lower flow deflections in each cascade. In both cases, however, the mean-line model shows excellent agreement with CFD simulations.

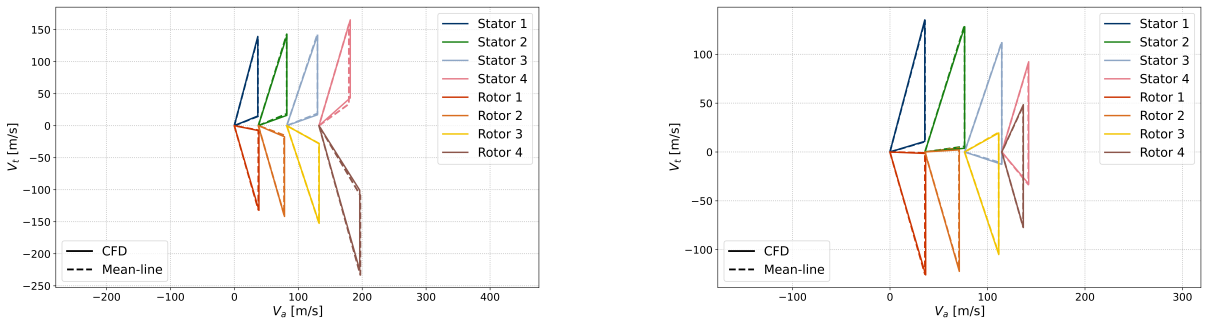

(a) Velocity triangles at $T_{amb} = 0$ °C

(b) Velocity triangles at $T_{amb} = 40$ °C

Figure 8: Comparison of velocity triangles at midspan in off-design conditions

4. CONCLUSIONS

This work has presented the development and validation of a mean-line model for the design and off-design analysis of ORC axial turbines. The design tool has been implemented to provide, also through the coupling with the genetic algorithm optimizer, a definition of an optimal expander flow path, performance and fluid-dynamic behaviour. The off-design tool enables, then, accurate performance predictions across a wide range of operating conditions. In the code, losses and deviations are estimated using the Aungier correlations, particularly suitable for ORC turbines, especially under transonic conditions. The Came target pressure method was integrated into the off-design model, ensuring an accurate prediction of the pressure ratio distribution along the machine and correctly identifying the stage where choking occurs.

The model was validated against CFD simulations using a test case representative of low-temperature mid-capacity geothermal power plant, operating with isobutane as working fluid. A dedicated post-processing strategy was employed to ensure a meaningful comparison, extracting mass-averaged flow properties and performance indicators. The results showed excellent agreement, with the mean-line model proven to accurately capture the thermodynamic quantities distribution, velocity triangles, and overall efficiency trends. Notably, the off-design analysis provides excellent estimation of the expander efficiency and very good estimate of flow rates and power, showing also high reliability in predicting transonic and supersonic conditions.

Future developments will focus on extending the validation to other fluid families, such as siloxanes and refrigerants, to assess the model's robustness across different working fluids. Further refinements will include the validation of clearance loss correlations, the extension to turbine architectures beyond the constant mean diameter configuration, and the integration of a diffuser model to predict the kinetic energy recovery in both design and off-design conditions. In addition, the integration of multi-point optimisation strategies will be explored, allowing the expander design to account for performance over a range of operating conditions rather than at a single design point.

REFERENCES

Ainley, D. and Mathieson, G. (1951). A method of performance estimation for axial-flow turbines. *Aeronautical Research Council Reports & Memoranda*.

Aungier, R. H. (2006). *Turbine Aerodynamics: Axial-Flow and Radial-Flow Turbine Design and Analysis*. ASME Press.

Bell, I. H., Wronski, J., Quoilin, S., and Lemort, V. (2014). Pure and pseudo-pure fluid thermophysical property evaluation and the open-source thermophysical property library coolprop. *Industrial & Engineering Chemistry Research*, 53(6):2498–2508.

Biscani, F. and Izzo, D. (2020). A parallel global multiobjective framework for optimization: pagmo. *Journal of Open Source Software*, 5(53):2338.

Came, P. M. (1995). Streamline curvature throughflow analysis of axial-flow turbines.

Craig, H. R. M. and Cox, H. J. A. (1970). Performance estimation of axial flow turbines. *Proceedings of the Institution of Mechanical Engineers*, 185(1):407–424.

Dunham, J. and Came, P. M. (1970). Improvements to the ainley-mathieson method of turbine performance prediction. *Journal of Engineering for Power*, 92(3):252–256.

Haghighi, A., Pakatchian, M., El Haj Assad, M., Duy, V., and Nazari, M. (2020). A review on geothermal organic rankine cycles: modeling and optimization. *Journal of Thermal Analysis and Calorimetry*, 144.

Jiménez-García, J. C., Ruiz, A., Pacheco-Reyes, A., and Rivera, W. (2023). A comprehensive review of organic rankine cycles. *Processes*, 11(7).

Kacker, S. C. and Okapuu, U. (1982). A mean line prediction method for axial flow turbine efficiency. *Journal of Engineering for Power*, 104(1):111–119.

Lemmon, E. W., Bell, I. H., Huber, M. L., and McLinden, M. O. (2018). NIST Standard Reference Database 23: Reference Fluid Thermodynamic and Transport Properties-REFPROP, Version 10.0, National Institute of Standards and Technology.

Macchi, E. (2017). Theoretical basis of the organic Rankine cycle. In *Organic Rankine Cycle (ORC) Power Systems*. Woodhead Publishing.

Mahmoudi, A., Fazli, M., and Morad, M. (2018). A recent review of waste heat recovery by organic rankine cycle. *Applied Thermal Engineering*, 143:660–675.

Manfredi, M., Persico, G., Dossena, V., Cosi, L., Forte, A., and Arcangeli, L. (2023). A strategy for the design of orc multi-stage axial turbines for geothermal energy conversion. In *Turbo Expo*, volume Volume 13B: Turbomachinery — Axial Flow Turbine Aerodynamics.

Zweifel, O. (1945). The spacing of turbo-machine blading, especially with large angular deflection. *Brown Boveri Rev.*, 32(12):436–444.